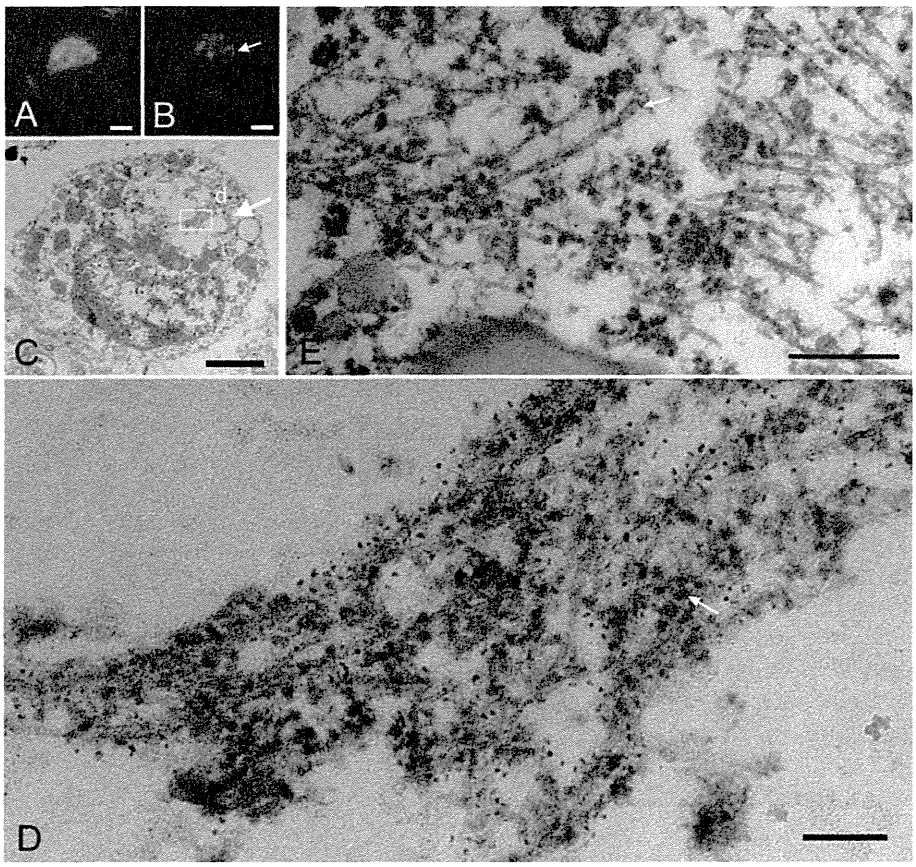

Figure 6 Correlation of immunolabeled LM and EM images of Pick-like inclusions in two CBD cases. A densely packed round inclusion (Pick-like inclusion) from a CBD case (case 3) labeled with anti-PHF antibody (AT8) visualized with QD 655, also labeled with Alexa 488 for more precise confocal images **(A)**. Correlated LM and EM images **(B, C)** showed that tau immunoreactivity around the cavity on LM corresponded to bundles of tau filaments that were not arranged as parallely as in AD (**C**, rectangle d; **D**). Note that these filaments were intermingled with ribosomes (**D**, arrow). **(E)** The ultrastructure of Pick-like inclusions in another case of CBD (case 4) also revealed randomly assembled tau filaments with occasional formation of paired helical filaments (a periodicity of 130 nm, arrow). Scale bars in **A** to **C** = 3 μm; **D** = 50 nm; **E** = 100 nm. **A** to **D**, case 3; **E**, case 4.

Table 2 Similarities and differences between AD-pretangle and CBD-pretangle

		AD		CBD	
		Pretanle	**NFT**	**Pretangle**	**Pick like inclusion**
LM findings (confocal images)	Morphology	Granular	Fibrillary	Reticular	Round, frequent vacuoles
	Perinuclear accentuation	Occiasional	Occasional	None	None
	Size of neurons involved	Small- to large- sized	Small- to large- sized	Medium- to large-sized	Small-sized
EM findings	Density of tau filaments	Very sparse*1	Very dense*2	Sparse	Dense
	Arrangement of tau filaments	Irregular/regular (focal NFT formation*3)	Regular (NFT formation)	Irregular	Irregular
	Diameter of straight filaments	About 15 nm	About 15 nm	14-20 nm	About 15 nm
	PHF (a periodicity)	Occasional (about 80 nm)	Frequent (about 80 nm)	None	Occasional (130–180 nm)

IHC, immunohistochemistry; LM, light microscopy; EM, electron microscopy; PHF, paired helical filaments; *1, Density of straight tau filament is more sparse in AD-pretangles than in CBD-pretangles; *2, Density of tau filaments is more dense in AD-NFT than in Pick-like inclusions of CBD; *3, NFT, neurofibrillary tangle signifying a regularly and tightly arranged bundle of straight or paired helical filaments.

to label the entire thickness of floating sections with QDs so that each tau filament was sufficiently labeled (Figures 3 and 4). Consequently, confocal images and immunoEM images could be tightly correlated.

Other disadvantages of QDs are that they have a lower electron density and less distinct contours than colloidal gold for immunolabeling. We previously used EDX spot analysis with STEM to demonstrate the presence of Se and Cd on a pixel basis [19]. This EDX spot analysis, now extended to map the entire EM field, resulted in clear visualization of the position and form of each QD particle. When the corresponding EM image was overlaid, QDs could be readily differentiated from the grayscale cellular backgrounds (e.g., ribosomes) (Figure 2). Similar elemental mapping of Cd has been reported using electron energy loss spectrography (EELS) to detect QDs in ultrathin EM samples [35]. However, compared with EELS, EDX is more suitable for the detection of heavy metals, such as Cd or Se [19,36]. Moreover, because EELS is performed without electron staining, it is difficult to gain sufficient contrast in EM images [35]. Therefore, combined with pre-embedding Q-dot immunoEM and EDX mapping, the use of QDs is one of the most sensitive and distinct ultrastructural immunolabeling techniques available and might be particularly suitable for the correlation of LM/EM images.

Conclusions

Accurate identification of pretangles on LM, followed by EM examination of their exact counterpart was achieved through tau immunolabeling with QD, fluorescent nanocrystals, which are detectable with LM (fluorescence signal) and with EM (electron dense particles with halo). EDX spot analysis to confirm the identity of QD on EM section by showing energy peaks for Cd and Se is now extended to map the entire EM field to highlight QD particles. This improved method with EDX mapping clearly demonstrated for the first time that AD-pretangles showed a strong tendency to form fibrillary tangles even at an early stage, whereas pretangles or Pick-like inclusions in tissue from patients with CBD did not even at an advanced stage. This novel strategy is useful to clarify how molecules other than tau are organized into ultrastructures in the early stages of disease-specific lesions.

Additional files

Additional file 1: Figure S1. Optimal of dilution of QD-conjugated secondary antibodies for ultrastruc-tural immunolabeling.

Additional file 2: Figure S2. Energry dispersive X-ray (EDX) mapping of Quantum dots (QDs).

Competing interests

The authors declare that they have no competing interests.

Authors' contributions

ST, TU, RT and MY designed the study, analysed the data, and drafted the manuscript. ST, TU, IA, YI, MM, MY collected clinical and pathological data. All authors read and approved the final manuscript.

Acknowledgments

This study was supported by Grants-in-Aid for Scientific Research (JSPS KAKENHI 25430057) from the Ministry of Education, Culture, Sports, Science and Technology; a grant from the Japan Foundation for Neuroscience and Mental Health, the Mitsui Life Social Welfare Foundation, and the Tokyo Metropolitan Institute of Medical Science project 'Mechanism for Early Diagnosis and Prevention of Parkinson's disease; and Grants-in-Aid from the Research Committee of CNS Degenerative Diseases, the Ministry of Health, Labour and Welfare of Japan. We are grateful to Takashi Kanemura (Hitachi High-Technologies Corporation) for excellent operation of EDX spot analysis and mapping. Technical contributions by Mr. Kentaro Endo, Ms. Hiromi Kondo (Histology Center) and Ms. Ayako Nakamura (Laboratory of Structural Neuropathology) at Tokyo Metropolitan Institute of Medical Science are gratefully acknowledged.

Author details

[1]Department of Neuropathology, Institute for Medical Science of Aging, Aichi Medical University, Nagakute, Aichi, Japan. [2]Laboratory of Structural Neuropathology, Tokyo Metropolitan Institute of Medical Science, 2-1-6 Kamikitazawa, Setagaya, Tokyo 156-8506, Japan. [3]Department of Neurology, Kyoto University, Kyoto, Japan. [4]Department of Neurology, Higashi Nagoya National Hospital, Nagoya, Aichi, Japan.

Received: 5 November 2014 Accepted: 5 November 2014
Published online: 11 December 2014

References

1. Ross CA, Poirier MA (2004) Protein aggregation and neurodegenerative disease. Nat Med 10(Suppl):S10–S17, doi:10.1038/nm1066
2. Bancher C, Grundke-Iqbal I, Iqbal K, Fried VA, Smith HT, Wisniewski HM (1991) Abnormal phosphorylation of tau precedes ubiquitination in neurofibrillary pathology of Alzheimer disease. Brain Res 539(1):11–18
3. Braak E, Braak H, Mandelkow EM (1994) A sequence of cytoskeleton changes related to the formation of neurofibrillary tangles and neuropil threads. Acta Neuropathol 87(6):554–567
4. Uchihara T (2014) Pretangles and neurofibrillary changes -Similarities and differences between AD and CBD based on molecular and morphological evolution. Neuropathology 34(6):571–7, doi:10.1111/neup.12108
5. Kidd M (1963) Paired helical filaments in electron microscopy of Alzheimer's disease. Nature 197:192–193
6. Dickson DW, Bergeron C, Chin SS, Duyckaerts C, Horoupian D, Ikeda K, Jellinger K, Lantos PL, Lippa CF, Mirra SS, Tabaton M, Vonsattel JP, Wakabayashi K, Litvan I (2002) Office of Rare Diseases neuropathologic criteria for corticobasal degeneration. J Neuropathol Exp Neurol 61(11):935–946
7. Uchihara T, Mitani K, Mori H, Kondo H, Yamada M, Ikeda K (1994) Abnormal cytoskeletal pathology peculiar to corticobasal degeneration is different from that of Alzheimer's disease or progressive supranuclear palsy. Acta Neuropathol 88(4):379–383
8. Tatsumi S, Mimuro M, Iwasaki Y, Takahashi R, Kakita A, Takahashi H, Yoshida M (2014) Argyrophilic grains are reliable disease-specific features of corticobasal degeneration. J Neuropathol Exp Neurol 73(1):30–38, doi:10.1097/NEN.0000000000000022
9. Watanabe S, Punge A, Hollopeter G, Willig KI, Hobson RJ, Davis MW, Hell SW, Jorgensen EM (2011) Protein localization in electron micrographs using fluorescence nanoscopy. Nat Methods 8(1):80–84, doi:10.1038/nmeth.1537
10. Modla S, Czymmek KJ (2011) Correlative microscopy: a powerful tool for exploring neurological cells and tissues. Micron 42(8):773–792, doi:10.1016/j.micron.2011.07.001
11. Jahn KA, Barton DA, Kobayashi K, Ratinac KR, Overall RL, Braet F (2012) Correlative microscopy: providing new understanding in the biomedical and plant sciences. Micron 43(5):565–582, doi:10.1016/j.micron.2011.12.004
12. Caplan J, Niethammer M, Taylor RM 2nd, Czymmek KJ (2011) The power of correlative microscopy: multi-modal, multi-scale, multi-dimensional. Curr Opin Struct Biol 21(5):686–693, doi:10.1016/j.sbi.2011.06.010

13. Giepmans BN, Deerinck TJ, Smarr BL, Jones YZ, Ellisman MH (2005) Correlated light and electron microscopic imaging of multiple endogenous proteins using Quantum dots. Nat Methods 2(10):743–749, doi:10.1038/nmeth791
14. Karreman MA, Agronskaia AV, van Donselaar EG, Vocking K, Fereidouni F, Humbel BM, Verrips CT, Verkleij AJ, Gerritsen HC (2012) Optimizing immuno-labeling for correlative fluorescence and electron microscopy on a single specimen. J Struct Biol 180(2):382–386, doi:10.1016/j.jsb.2012.09.002
15. Deerinck TJ (2008) The application of fluorescent quantum dots to confocal, multiphoton, and electron microscopic imaging. Toxicol Pathol 36(1):112–116, doi:10.1177/0192623307310950
16. Cortese K, Diaspro A, Tacchetti C (2009) Advanced correlative light/electron microscopy: current methods and new developments using Tokuyasu cryosections. J Histochem Cytochem 57(12):1103–1112, doi:10.1369/jhc.2009.954214
17. Faas FG, Barcena M, Agronskaia AV, Gerritsen HC, Moscicka KB, Diebolder CA, van Driel LF, Limpens RW, Bos E, Ravelli RB, Koning RI, Koster AJ (2013) Localization of fluorescently labeled structures in frozen-hydrated samples using integrated light electron microscopy. J Struct Biol 181(3):283–290, doi:10.1016/j.jsb.2012.12.004
18. Heines MA, Guyot-Sionnest P (1996) Synthesis and characterization of strongly luminsecing ZnS-capped CdSe nanocrystals. J Phys Chem 100:468–471
19. Uematsu M, Adachi E, Nakamura A, Tsuchiya K, Uchihara T (2012) Atomic identification of fluorescent Q-dots on tau-positive fibrils in 3D-reconstructed pick bodies. Am J Pathol 180(4):1394–1397, doi:10.1016/j.ajpath.2011.12.029
20. Kanazawa T, Adachi E, Orimo S, Nakamura A, Mizusawa H, Uchihara T (2012) Pale neurites, premature alpha-synuclein aggregates with centripetal extension from axon collaterals. Brain Pathol 22(1):67–78, doi:10.1111/j.1750-3639.2011.00509.x
21. Montine TJ, Phelps CH, Beach TG, Bigio EH, Cairns NJ, Dickson DW, Duyckaerts C, Frosch MP, Masliah E, Mirra SS, Nelson PT, Schneider JA, Thal DR, Trojanowski JQ, Vinters HV, Hyman BT (2012) National Institute on Aging-Alzheimer's Association guidelines for the neuropathologic assessment of Alzheimer's disease: a practical approach. Acta Neuropathol 123(1):1–11, doi:10.1007/s00401-011-0910-3
22. Takahashi T, Amano N, Hanihara T, Nagatomo H, Yagishita S, Itoh Y, Yamaoka K, Toda H, Tanabe T (1996) Corticobasal degeneration: widespread argentophilic threads and glia in addition to neurofibrillary tangles. Similarities of cytoskeletal abnormalities in corticobasal degeneration and progressive supranuclear palsy. J Neurol Sci 138(1–2):66–77
23. Arima K, Uesugi H, Fujita I, Sakurai Y, Oyanagi S, Andoh S, Izumiyama Y, Inose T (1994) Corticonigral degeneration with neuronal achromasia presenting with primary progressive aphasia: ultrastructural and immunocytochemical studies. J Neurol Sci 127(2):186–197
24. Feany MB, Dickson DW (1995) Widespread cytoskeletal pathology characterizes corticobasal degeneration. Am J Pathol 146(6):1388–1396
25. Ksiezak-Reding H, Morgan K, Mattiace LA, Davies P, Liu WK, Yen SH, Weidenheim K, Dickson DW (1994) Ultrastructure and biochemical composition of paired helical filaments in corticobasal degeneration. Am J Pathol 145(6):1496–1508
26. Mori H, Nishimura M, Namba Y, Oda M (1994) Corticobasal degeneration: a disease with widespread appearance of abnormal tau and neurofibrillary tangles, and its relation to progressive supranuclear palsy. Acta Neuropathol 88(2):113–121
27. Lippa CF, Smith TW, Fontneau N (1990) Corticonigral degeneration with neuronal achromasia. A clinicopathologic study of two cases. J Neurol Sci 98(2–3):301–310
28. Wakabayashi K, Oyanagi K, Makifuchi T, Ikuta F, Homma A, Homma Y, Horikawa Y, Tokiguchi S (1994) Corticobasal degeneration: etiopathological significance of the cytoskeletal alterations. Acta Neuropathol 87(6):545–553
29. Kato S, Nakamura H, Otomo E (1989) Reappraisal of neurofibrillary tangles. Immunohistochemical, ultrastructural, and immunoelectron microscopical studies. Acta Neuropathol 77(3):258–266
30. Lowe J, Mirra SS, Hyman B, Dickson DW (2008) Histopathology of Alzheimer's disease. In: Love S, Louis DN, Ellison DW (eds) Greenfield's neuropathology, vol 1, 8th edn. Edward Arnold, London, pp 1031–1152
31. Metuzals J, Robitaille Y, Houghton S, Gauthier S, Leblanc R (1988) Paired helical filaments and the cytoplasmic-nuclear interface in Alzheimer's disease. J Neurocytol 17(6):827–833
32. Hara M, Hirokawa K, Kamei S, Uchihara T (2013) Isoform transition from four-repeat to three-repeat tau underlies dendrosomatic and regional progression of neurofibrillary pathology. Acta Neuropathol 125(4):565–579, doi:10.1007/s00401-013-1097-6
33. Andorfer C, Acker CM, Kress Y, Hof PR, Duff K, Davies P (2005) Cell-cycle reentry and cell death in transgenic mice expressing nonmutant human tau isoforms. J Neurosci 25(22):5446–5454, doi:10.1523/JNEUROSCI. 4637-04.2005
34. Yang Y, Geldmacher DS, Herrup K (2001) DNA replication precedes neuronal cell death in Alzheimer's disease. J Neurosci 21(8):2661–2668
35. Nisman R, Dellaire G, Ren Y, Li R, Bazett-Jones DP (2004) Application of quantum dots as probes for correlative fluorescence, conventional, and energy-filtered transmission electron microscopy. J Histochem Cytochem 52(1):13–18
36. Leapman RD, Ornberg RL (1988) Quantitative electron energy loss spectroscopy in biology. Ultramicroscopy 24(2–3):251–268

doi:10.1186/s40478-014-0161-3
Cite this article as: Tatsumi *et al.*: Ultrastructural differences in pretangles between Alzheimer disease and corticobasal degeneration revealed by comparative light and electron microscopy. *Acta Neuropathologica Communications* 2014 **2**:161.

J Neuropathol Exp Neurol

Vol. 73, No. 12
December 2014
pp. 1183–1190

ORIGINAL ARTICLE

Early Pathologic Changes in Hereditary Diffuse Leukoencephalopathy With Spheroids

Yuichi Riku, MD, Takashi Ando, MD, Yoji Goto, MD, Kazuo Mano, MD, Yasushi Iwasaki, MD, Gen Sobue, MD, and Mari Yoshida, MD

Abstract

Hereditary diffuse leukoencephalopathy with spheroids (HDLS) is a familial neurodegenerative disease clinically characterized by progressive cognitive and motor dysfunction. Mutations in the colony-stimulating factor 1 receptor (*CSF1R*) gene have recently been identified in HDLS patients. The presence of diffuse axonal spheroids, myelin loss, and pigmented microglia in the white matter are pathologic hallmarks of HDLS; however, early pathologic findings have not been described in HDLS patients. We report a Japanese family with HDLS. A novel heterozygous c.653 C>Y mutation in the *CSF1R* gene was identified in the female proband who died at the age of 63 years; postmortem findings were compatible with HDLS. We also autopsied her sister who was considered to be neurologically asymptomatic and died of tuberculosis at the age of 44 years. Postmortem studies revealed patchy axonal degeneration and myelin loss, predominantly in the subcortical white matter. Pigmented microglia were distributed diffusely throughout the cerebral white matter and expressed CSF1R poorly. In conclusion, our observations suggest that the pathology of HDLS may initially be characterized by multifocal lesions in subcortical white matter regions. Moreover, pigmented microglia poorly express CSF1R and are distributed diffusely throughout the white matter at the early disease stage, preceding axonal damage and myelin loss.

Key Words: Autopsy, Axonal spheroids, *CSF1R* gene, Hereditary diffuse leukoencephalopathy with spheroids, Leukoencephalopathy, MRI, Pigmentary leukodystrophy.

INTRODUCTION

Hereditary diffuse leukoencephalopathy with spheroids (HDLS) is a familial neurodegenerative disease that causes progressive cognitive and motor dysfunction (1,2). The onset of neurologic manifestations in the fourth or fifth decade, progressing to dementia and then death within a decade, is typical of HDLS (2–4). The core manifestations of HDLS are behavioral changes, depression, dementia, motor impairment, and epilepsy (2–5). In 2012, mutations of the colony-stimulating factor 1 receptor (*CSF1R*) gene were reported to be causative of HDLS (6). Neuropathologically, HDLS is characterized by diffuse loss of myelin and the presence of axonal spheroids and pigmented microglia throughout the white matter of the brain (4,5). However, the early pathologic changes in HDLS have remained unclear because patients have usually been autopsied at advanced stages of the disease. Thus, the pathologic processes contributing to the formation of the observed white matter lesions are unknown.

Here, we report a Japanese family with HDLS, among whom 2 patients were autopsied. The female proband experienced a disorder that was clinically and genetically consistent with HDLS, survived for 16 years after disease onset, and was autopsied after her death at the age of 63 years. We also autopsied her sister who had been considered to be neurologically asymptomatic and who incidentally died of tuberculosis. Intriguingly, postmortem examination of this sibling revealed pathologic changes observed in HDLS. We discuss early and late-stage pathologic characteristics of HDLS based on comparative observations of these 2 patients.

MATERIALS AND METHODS

Clinical and Genetic Studies

Written informed consent was obtained from family members to archive tissues for clinical, genetic, and pathologic analyses. Standard neurologic examinations, Mini-Mental State Examinations, neuroimaging, and family history collection were performed by neurologic experts at Nagoya Daiichi Red Cross Hospital. Analyses of the *CSF1R* gene were performed using frozen brain tissue. We previously reported the methods and results of genetic analyses of this kindred (7).

Neuropathologic Evaluations

The brains and spinal cords were fixed in 20% neutral buffered formalin. Samples obtained from several regions of the brain and spinal cord were embedded in paraffin; sectioned at a thickness of 4.5 μm; mounted on slides; and stained with hematoxylin and eosin, Klüver-Barrera, Holzer, toluidine blue, and periodic acid Schiff stains. Von-Kossa staining was also performed to detect tissue calcification. Immunohistochemical studies were performed on 4.5-μm-thick sections using ENVISION kits (Dako, Glostrup, Denmark)

From the Department of Neurology, Nagoya University Graduate School of Medicine (YR, GS), Aichi, Japan; and Department of Neurology, Nagoya Daiichi Red Cross Hospital (TA, YG, KM), Aichi, Japan; and Institute for Medical Science of Aging, Aichi Medical University (YI, MY), Aichi, Japan.
Send correspondence and reprint requests to: Mari Yoshida, MD, Institute for Medical Science of Aging, Aichi Medical University, Yazakokarimata 9, Nagakute, Aichi, Japan; E-mail: myoshida@aichi-med-u.ac.jp
This study was supported by Grants-in-Aid from the Research Committee for CNS Degenerative Diseases, Ministry of Health, Labour and Welfare, Japan.
All authors report no conflict of interest.

with diaminobenzidine ([DAB] Wako, Osaka, Japan) as a brown chromogen. The primary antibodies used were anti-ubiquitin (polyclonal rabbit, 1:2000; Dako), anti-CSF1R (polyclonal rabbit, 1:200; Santa Cruz Biotechnology, Dallas, TX), anti–β-amyloid peptide (6 F/3D, monoclonal mouse, 1:200; Dako), phosphorylated tau ([p-tau] AT8, monoclonal mouse, 1:2000; Innogenetics, Zwijndrecht, Belgium), anti-neurofilament (2 F11, monoclonal mouse, 1:600; Dako), anti-SMI31 (monoclonal mouse, 1:1000; Covance, San Diego, CA), and anti–amyloid protein precursor (polyclonal rabbit, 1:1000; StressGen, San Diego, CA). Anti-CD68 (immunohistochemistry: monoclonal mouse, 1:200; Dako; immunoblot: polyclonal rabbit, 1:1000; Santa Cruz Biotechnology) and anti-Iba1 (immunohistochemistry: polyclonal rabbit, 1:1000; Wako) were used as microglial markers. To compare the distributions of pigmented microglia and axonal spheroids, double-staining immunohistochemistry was used to visualize CD68 and neurofilaments using DAB and the VIP Peroxidase Substrate Kit (SK-4600; Vector Laboratories, Burlingame, CA) as brown and violet chromogens, respectively. For electron microscopy, cerebral white matter sections were fixed in 4% glutaraldehyde. The sections were washed in phosphate buffer, postfixed with osmium tetroxide, dehydrated in ethanol, and embedded in Epon. Ultrathin sections were stained with uranyl acetate and lead citrate and examined by electron microscopy.

Analysis of CSF1R Protein Expression on Microglia

Recently, a perturbation of CSF1R signaling by a dominant-negative mechanism has been reported to play a role in the pathogenesis of HDLS (8). We analyzed CSF1R protein expression on pigmented microglia by examining CD68 and CSF1R by double immunofluorescence and Western blot. Control tissue for double immunofluorescence studies was prepared from the brain of a 65-year-old man with Binswanger disease; this control was chosen because microglia are abundant in the white matter of Binswanger disease patients but would be too sparse in normal brains to evaluate by immunohistochemistry. Cerebral white matter sections, 4.5-μm thick, were incubated in a mixture of anti-CD68 (1:100) and anti-CSF1R (1:100) antibodies for 3 hours after antigen retrieval accomplished using trypsin. The sections were then labeled with secondary antibodies against mouse IgG (Alexa Fluor 488; Molecular Probes, Carlsbad, CA) and rabbit IgG (Alexa Fluor 565; Molecular Probes) for 2 hours.

Western Blot

To confirm our immunohistochemical results, we also examined CD68 and CSF1R by Western blot using tissue from the proband; frozen tissues were available only from this individual. Proteins from the frontal cortex of the patient and a control subject were extracted and fractionated as previously described (8). Detergent-extracted lysates were subjected to sodium dodecyl sulfate polyacrylamide gel electrophoresis followed by immunoblotting. A rabbit polyclonal antibody against CD68 (1:1000) was used as a microglial marker. A polyclonal anti-CSF1R antibody (1:1000) was used to detect CSF1R. To study CSF1R expression relative to CD68 expression, we adjusted sample volumes on the basis of the CD68 band signal strength and reperformed a Western blot.

RESULTS

Clinical History

Proband (Patient II-1)

The proband had been healthy and normally intelligent until the age of 48 years, at which time she began to exhibit forgetfulness about recent events and to have difficulty understanding daily conversation and calculations; she then had to quit her job. She bought the same items repeatedly and was not able to insert train tickets into a ticket machine in the proper direction. At the age of 49 years, she was admitted to our hospital after a generalized seizure. After recovering from the seizure, a neurologic examination revealed severe amnesia, apathy, aphasia, apraxia, and spastic tetraplegia predominantly in the right limbs. The patient's Mini-Mental State Examinations score was 0/30 points because she was only able to say the words "yes" or "no." T2-weighted magnetic resonance imaging (MRI) imaging (T2WI) showed multiple hyperintense lesions in the cerebral white matter (Fig. 1A). Tc99m-ECD single-photon emission computed tomography revealed hypoperfusion in the frontal and parietal lobes, but perfusion of the basal ganglia and the cerebellum was relatively spared. Diffuse theta waves over the cerebrum were observed on an electroencephalogram. Analyses of the patient's blood and cerebrospinal fluid revealed no abnormalities. Thereafter, her neuropsychiatric and neurologic symptoms rapidly progressed, and her epileptic seizures became refractory. At the age of 50 years, she was completely bedridden because of spastic tetraplegia. At the age of 56 years, MRI revealed diffuse and severe atrophy in the white matter, with marked dilatation of the lateral and third ventricles (Fig. 1B). Marked and diffuse hypoperfusion of the cerebral cortices were observed by Tc99m-ECD–single-photon emission computed tomography. The patient died of aspiration pneumonia at the age of 63 years. We autopsied the patient after obtaining informed consent from her family members. Genetic analysis was performed using frozen brain tissue obtained at autopsy; sequence analysis of the patient's polymerase chain reaction–amplified DNA revealed a novel heterozygous c.653 C>Y mutation in the *CSF1R* gene (7).

Sibling II-2

The proband's sister presented with gradual apathy, depression, and repetitive behavior at the age of 42 years. At the age of 43 years, a neurologic examination revealed marked apathy, moderate amnesia, and aphasia. Her Mini-Mental State Examinations score was 17/30. An electroencephalogram revealed diffuse theta waves over the cerebrum. An MRI scan showed mild ventricular dilatation with T2WI-hyperintense lesions in the deep cerebral white matter indicative of HDLS (Fig. 1C). She gradually became bedridden because of spasticity and weakness of the limbs and died of bronchopneumonia at the age of 47 years. An autopsy was not performed.

Sibling II-3

At the age of 44 years, another sister of the proband was admitted to our hospital because of miliary tuberculosis. Before

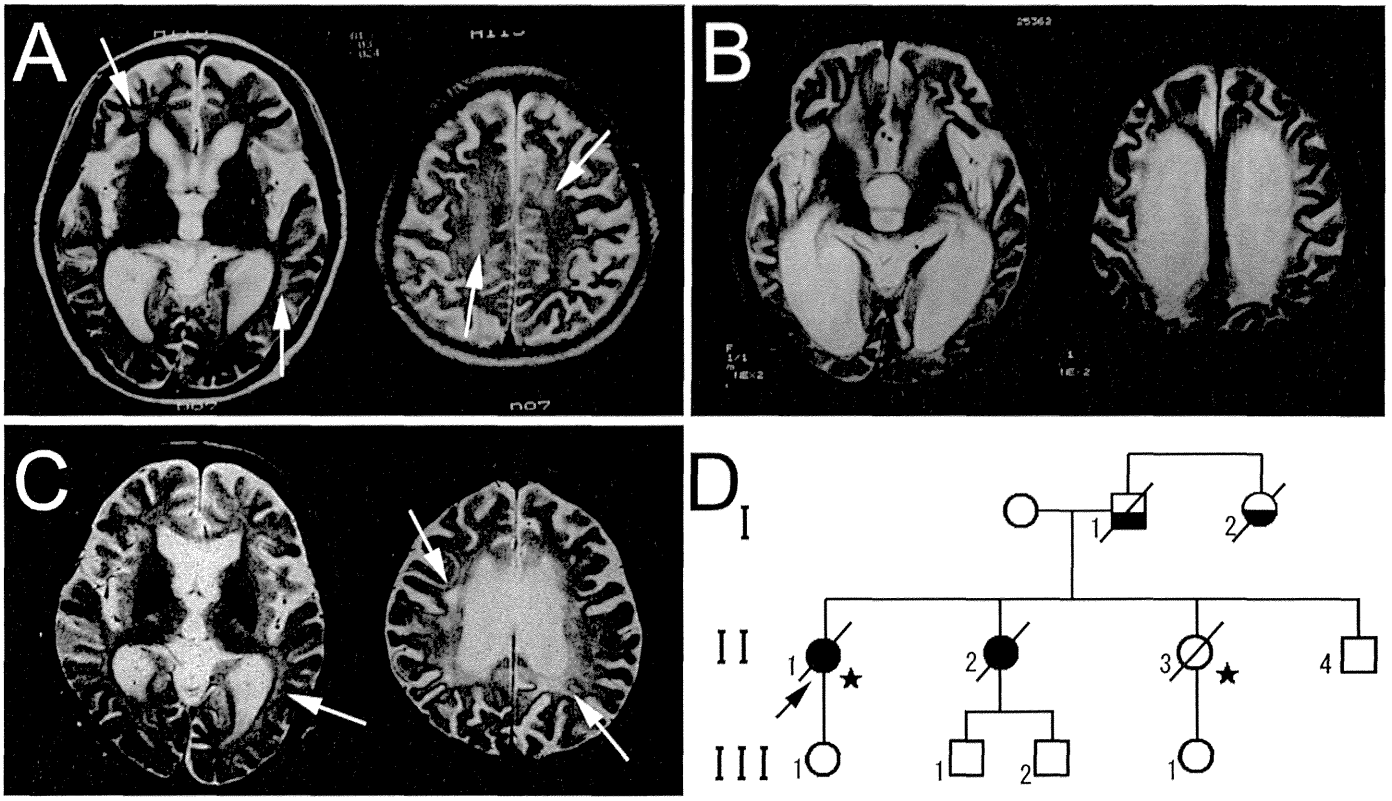

FIGURE 1. Magnetic resonance imaging and simplified pedigree of the present kindred. **(A)** T2-weighted images (T2-WI) of Patient II-1 (proband) at the age of 49 years showed asymmetric and multiple high-intensity areas (HIAs) in the frontal white matter. **(B)** At the age of 56 years, her cerebral white matter showed marked atrophy and diffuse symmetric T2-HIAs with dilatation of the lateral and third ventricles. **(C)** T2-WI of Sibling II-2 at the age of 43 years showed mild ventricular dilatation with hyperintense lesions in the deep cerebral white matter. **(D)** Simplified pedigree. Patient II-1 was the proband (arrows); Sibling II-2 was also clinically affected. Siblings II-3 and II-4 were considered to be neurologically asymptomatic. Generations are numbered with Roman numerals and individuals with Arabic numerals. Circles represent females and squares represent males. Solid symbols indicate clinically affected family members; half-solid symbols indicate family members who were likely affected. Slashes indicate dead family members; stars indicate individuals whose brains were autopsied.

admission, she had been doing well as a housewife, although chronic fatigue had set in 3 months before and had become persistent. On admission, she was suffering from severe dyspnea and fatigue. Neurologic examinations did not reveal dementia, weakness, pyramidal signs, extrapyramidal signs, or ataxia. She received antibiotic therapy but died of respiratory failure 3 weeks after admission. After obtaining informed consent from her family members, an autopsy was performed.

Other Family Members

According to the patients' family members, the patients' father and his sister had both suffered from rapidly progressive dementia with an onset in the fourth decade and had died in their fifth and fourth decades, respectively. The pedigree of the patients' kindred is summarized in Figure 1D.

Neuropathologic Findings

Postmortem tissues from the proband (Patient II-1) and Sibling II-3 were examined.

Proband (Patient II-1)

The brain weighed 885 g. Grossly, the cerebral white matter was severely atrophied and the lateral ventricles were markedly dilated. On sections, the cerebral white matter (Fig. 2A), the pyramidal tract in the medulla oblongata, and the lateral columns of the spinal cord appeared gelatinous. Klüver-Barrera staining revealed diffuse marked loss of myelin in the cerebral white matter (Fig. 2B) and the corticospinal tracts. The U-fibers were affected severely but partially spared. Holzer staining revealed diffuse gliosis in the white matter (Fig. 2C). The cerebellar white matter showed milder myelin loss versus the cerebrum and the corticospinal tracts. The cerebellar myelin loss was prominent in the folial white matter of the hemisphere, the ventral deep white matter, the hilum of the dentate nucleus, and the middle cerebellar peduncle but sparse in the cerebellar vermis and the superior cerebellar peduncle. On microscopic examination, the white matter of the brain and spinal cord showed loss of axon and myelin, axonal spheroids, and periodic acid Schiff–positive pigmented microglia (Fig. 2D, E). The axonal spheroids and pigmented microglia were most abundant in the cerebellum but rather sparse in severely damaged regions, including the frontal and parietal lobes. Calcification was often observed in the white matter and was prominent in the periventricular region. Calcification was abundant in strongly affected white matter regions but was found only rarely in vascular walls, gray matter, or mildly

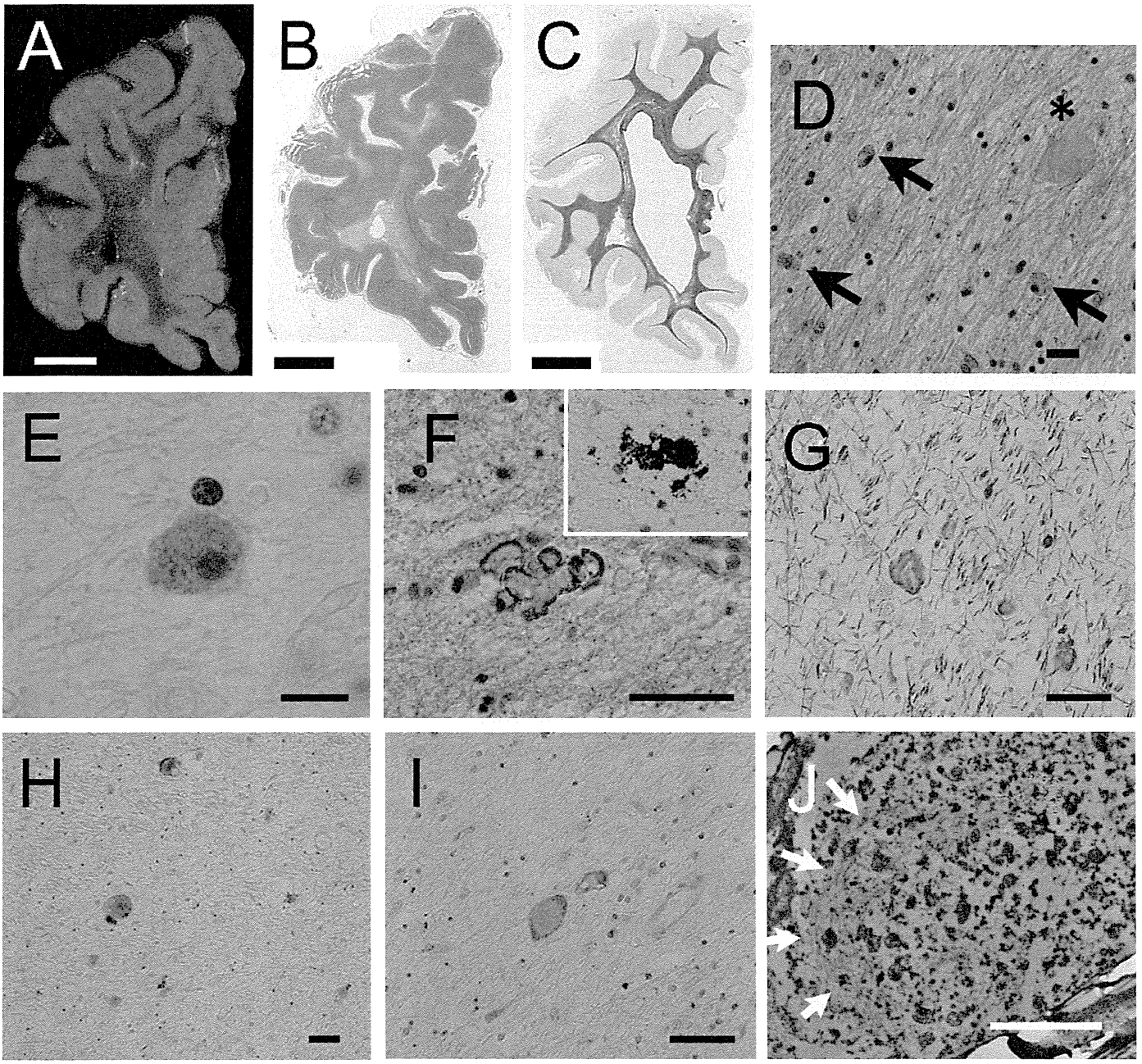

FIGURE 2. Postmortem observations of the proband. **(A)** A coronal section of the frontal lobe shows gelatinous degeneration of the white matter. **(B)** Myelin pallor and the destruction of the white matter were marked. The U-fibers were also depleted but partially spared. **(C)** Holzer staining revealed diffuse gliosis in the white matter. **(D)** The cerebellar white matter contained pigmented microglia (arrows) and axonal spheroids (asterisks). **(E)** A pigmented microglial cell was positive for periodic acid Schiff (PAS) staining. **(F)** Calcification was often observed within the white matter (inset shows von-Kossa staining). **(G–I)** The axonal spheroids were positive for SMI 31 **(G)**, amyloid protein precursor **(H)**, and ubiquitin **(I)** by immunohistochemistry. **(J)** On electron microscopy, axonal spheroids were found to contain peripheral bundles of neurofilaments (arrows) surrounding mitochondria and unspecified electron-dense material. Scale bars = **(A–C)** 1 cm; **(D, F–I)** 50 μm; **(E)** 10 μm; **(J)** 2 μm. Original magnification: **(A–C)** 1×; **(D, F–I)** 200×; **(E)** 1,000×; **(J)** 6,000×. **(B)** Klüver-Barrera; **(C)** Holzer; **(D, F)** hematoxylin and eosin; **(E)** PAS (inset in **F**) von-Kossa; **(G)** anti-SMI 31; **(H)** anti–amyloid protein precursor; **(I)** anti-ubiquitin immunostaining.

affected white matter regions (Fig. 2F). The axonal spheroids were 20 to 50 μm in diameter and stained for SMI 31 (Fig. 2G), amyloid protein precursor (Fig. 2H), and ubiquitin (Fig. 2I) by immunohistochemistry. Electron microscopic examination of the axonal spheroids revealed a neurofilament bundle surrounding the periphery of each dystrophic axon, which contained mitochondria and nonspecific electron-dense inclusions (Fig. 2J). Neuronal loss was not obvious in the cerebral cortices, basal ganglia, and spinal cord. In the brainstem, the substantia nigra showed mild extraneuronal melanin. The red

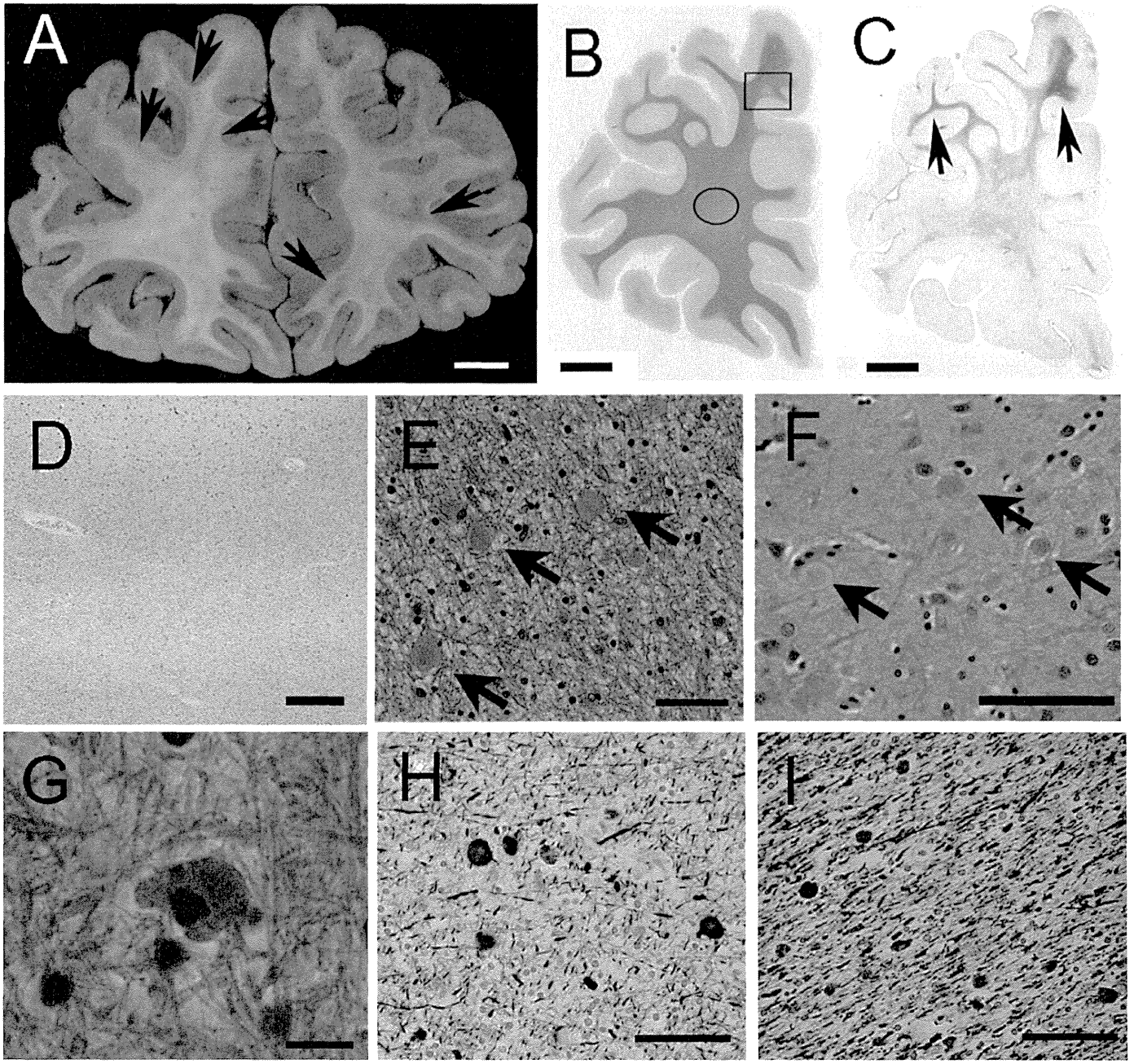

FIGURE 3. Postmortem observations of Sibling II-3. **(A)** Brownish discoloration was observed predominantly in the subcortical white matter (arrows). **(B, C)** Focal myelin pallor and gliosis were observed in the subcortical white matter (square in **B** and arrows in **C**). **(D)** Microscopically, the subcortical white matter exhibited band-shaped patterns of demyelination. **(E, F)** Axonal spheroids within subcortical regions of cerebral white matter (**E**, arrows) and adjacent deep cortical layers (**F**, arrows) are shown. **(G)** White matter also contained pigmented microglia. **(H, I)** Double immunohistochemical staining for CD68 (brown) and neurofilaments (dark violet) of the frontal white matter shows that CD68-positive microglia were more abundant in normal-appearing white matter (**I**, corresponding to the circled region in **B**) than in lesions with axonal degeneration (**H**, corresponding to the squared region in **B**). Scale bars = **(A–C)** 1 cm; **(D)** 500 μm; **(E, F, H, I)** 50 μm; **(G)** 10 μm. Original magnification = **(A–C)** 1×; **(D)** 40×; **(E, H, I)** 200×; **(F)** 400×; **(G)** 1,000. **(B, C)** Klüver-Barrera staining; **(D)** Holzer staining; **(E–G)** hematoxylin and eosin staining; **(H, I)** double immunohistochemistry examining both CD68 and neurofilaments.

nucleus, the pontine nuclei, the reticular formation, the inferior olivary nucleus, and the dorsal column nuclei showed only mild gliosis. Other gray matter of the brainstem including the peri-aqueductal gray matter, the locus coeruleus, the raphe nuclei, the dorsal nucleus of vagus, and the motor nuclei of the oculomotor, facial, and hypoglossal nerves appeared normal. The Purkinje cells and the granule cells of the cerebellar hemisphere and the vermis were spared, although the dentate nucleus showed mild gliosis. In addition, AT-8 immunohistochemistry revealed that the transentorhinal cortex and the hippocampus contained

several neurofibrillary tangles, corresponding to Braak stage II (9). No metachromatic material was present on staining with toluidine blue.

Sibling II-3

The brain weighed 1,330 g. The gross appearance of the brain surface appeared normal, but coronal sections of the cerebrum revealed multiple, band-shaped, brownish discolorations in the subcortical white matter of the frontal, temporal, and parietal lobes (Fig. 3A). Subcortical white matter showed focal myelin loss and gliosis with Klüver-Barrera and Holzer staining, respectively (Fig. 3B–D). Microscopic observation revealed pigmented microglia, axonal spheroids, and myelin loss predominantly in the frontal and parietal lobes (Fig. 3E–G). The axonal spheroids were multifocally distributed in subcortical regions of the cerebral white matter and adjacent deep cortical layers; however, pigmented microglia were spread relatively evenly throughout the white matter. Double immunohistochemistry for CD68 and neurofilament revealed that the burden of CD68-positive microglia was greater in normal-looking white matter rather than in white matter regions exhibiting axonal loss and spheroids (Fig. 3H, I). Neurons of the cerebral cortex, the basal ganglia, the gray matter in the brainstem, and the cerebellar cortex and dentate nucleus were generally preserved. Calcification was rarely observed in subcortical white matter. No additional pathologic changes were observed in the

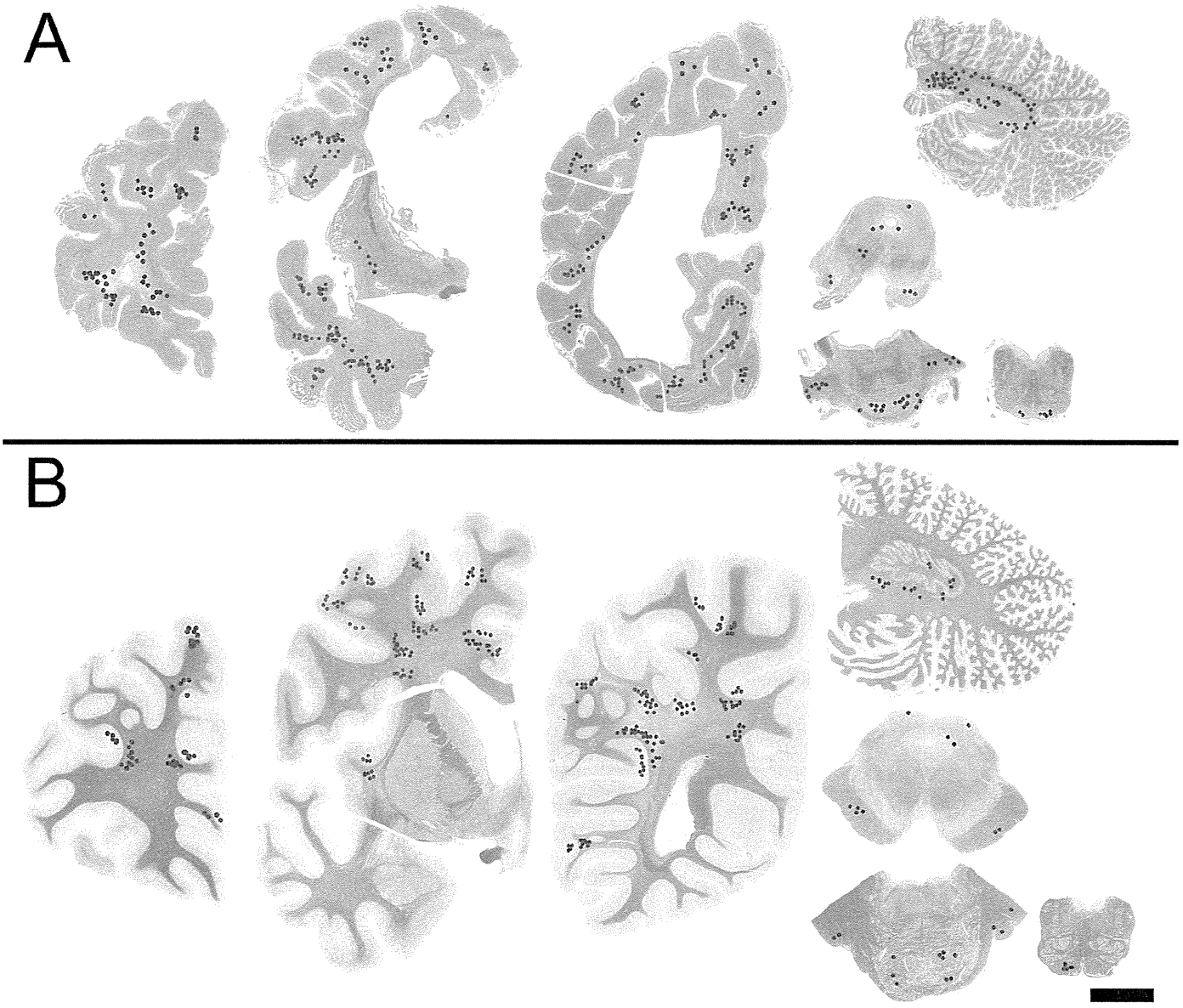

FIGURE 4. The distributions of axonal spheroids in Patients II-1 and II-3. **(A)** In Patient II-1, the axonal spheroids were diffusely distributed throughout the cerebral white matter. The axonal spheroids were sparse in highly affected regions. **(B)** In Patient II-3, myelin loss and axonal spheroids were observed focally and discontinuously, predominantly in the subcortical regions and adjacent deep cortical layers. Each red dot corresponds to a cluster of approximately 5 axonal spheroids. Klüver-Barrera staining. Scale bar = 1 cm. Original magnification: 1×.

brain. The distributions of axonal spheroids in Patients II-1 and II-3 are shown in Figure 4.

Analysis of CSF1R Protein Expression on Microglia

Double immunofluorescence for CD68 and CSF1R in Patient II-1 and Sibling II-3 demonstrated that CSF1R was expressed at lower levels in the patients' CD68-positive microglia than in control (Fig. 5A). Western blot analysis of CSF1R expression revealed approximately 130- and 160-kDa bands corresponding to monomeric CSF1R in control samples. In contrast, the 130- and 160-kDa CSF1R bands were less detectable in the samples from patient II-1; nevertheless, CD68 (~52–76 kDa) was detected at similar levels in both patient and control samples (Fig. 5B).

DISCUSSION

We have investigated a Japanese family with HDLS. The proband and one of her sisters presented with progressive neurologic deficits including amnesia, apathy, apraxia, epileptic seizures, and spastic paralysis, which were consistent with previous descriptions of HDLS (2,5,10). In contrast, another sister was considered to be neurologically asymptomatic before death but exhibited pathologic changes observed with HDLS. The present kindred exhibited apparent autosomal dominant inheritance of the disorder. Hereditary diffuse leukoencephalopathy with spheroids is usually an autosomal dominant disorder, although several sporadic patients who presented with leukoencephalopathy with axonal spheroids and pigmented microglia have been reported (11,12).

Importantly, the patient who was considered to be neurologically asymptomatic exhibited mild but definite white matter involvement (3,5,13,14). Multifocal axonal spheroids and myelin loss, associated with a brown discolored appearance, were observed in the white matter and were prominent in subcortical regions and in the adjacent deep layers of the cerebral cortices. A recent MRI observation at an early stage of disease revealed multiple asymmetric and multiple T2WI areas of high intensity in the cerebral white matter, suggesting that there may initially be multifocal and patchy white matter lesions and that these lesions may then become confluent as the disease progresses (3,4,15). Another study reported that on diffusion-weighted MRI, high signal bands with low apparent diffusion coefficients were observed in subcortical white matter regions in the early phases of the disease (16). These neuroimaging findings are consistent with the distributions of white matter discoloration, axonal spheroids, and myelin loss that we observed in this asymptomatic patient.

White matter calcification has recently been described in HDLS patients (8). In agreement with that finding, we observed

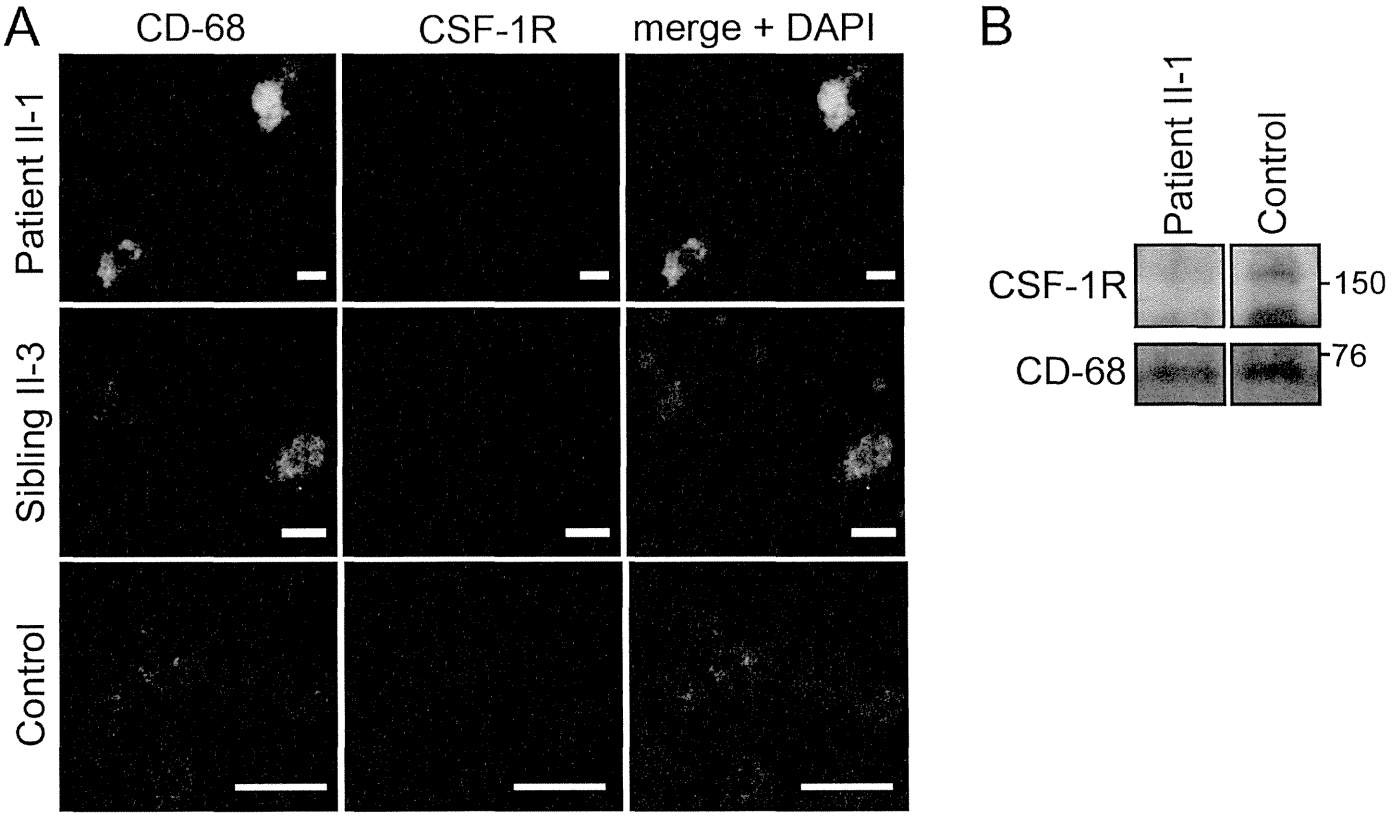

FIGURE 5. CSF1R expression on microglia. Double immunofluorescence examining CD68 (green) and CSF1R (red) reveals that CSF1R was less detectable on the patients' CD68-positive microglia in white matter versus control tissues. Control tissue was from a 65-year-old man with Binswanger disease. Nuclei were stained with 4′,6-diamidino-2-phenylindole, dihydrochloride. Scale bar = 25 μm. Original magnification: 400×. (**B**) Immunoblots showing CD68 and CSF1R. Approximately 130- and 160-kDa CSF1R bands were detected in the control sample and are undetectable in Patient II-1 sample. CD68 (~52–76 kDa) was detected similarly in both the patient and in the control samples.